



<https://doi.org/10.1038/s42003-025-08201-w>

Object fine-grained discrimination as a sensitive cognitive marker of transentorhinal integrity

Emma Delhaye^{1,2,3} , Gabriel Besson^{4,5}, Mohamed Ali Bahri¹ & Christine Bastin^{1,2} 

The transentorhinal cortex (tErC) is one of the first regions affected by Alzheimer's disease (AD), often showing changes before clinical symptoms appear. Understanding its role in cognition is key to detecting early cognitive impairments in AD. This study tested the hypothesis that the tErC supports fine-grained representations of unique individual objects, sensitively to the granularity of the demanded discrimination, influencing both perceptual and mnemonic functions. We examined the tErC's role in object versus scene discrimination, using objective (based on a pretrained convolutional neural network, CNN) and subjective (human-rated) measures of visual similarity. Our results show that the structural integrity of the tErC is specifically related to the sensitivity to visual similarity for objects, but not for scenes. Importantly, this relationship depends on how visual similarity is measured: it appears only when using CNN visual similarity measures in perceptual discrimination, and solely when using subjective similarity ratings in mnemonic discrimination. Furthermore, in mnemonic discrimination, object sensitivity to visual similarity was specifically associated with the integrity of tErC-BA36 connectivity, only when similarity was computed from subjective ratings. Altogether, these findings suggest that discrimination sensitivity to object visual similarity may represent a specific marker of tErC integrity after accounting for the type of similarity measured.

Alzheimer's disease (AD) neuropathology is characterised by neurofibrillary tau tangles and abnormal accumulation of amyloid- β (A β) plaques, progressing along a typical topographical route. A β accumulates from stage 1 in medial parietal structures, connected to the hippocampus via the entorhinal cortex. Several years before A β accumulation, neurofibrillary tau deposits start in the medial temporal lobe (MTL), specifically in the transentorhinal cortex (tErC), encompassing the medial portion of the perirhinal cortex (Brodmann area (BA) 35) and the antero-lateral portion of the entorhinal cortex (alErC)¹. These deposits then extend to other regions of the MTL including the hippocampus^{2–4}. Tau deposits have been associated with concomitant cell loss and neuronal atrophy in the respective brain regions in incipient AD^{3,5–8}.

In addition, AD affects the dense pattern of resting-state functional connectivity typically described within the MTL itself⁹, as well as between the MTL and other cortical and subcortical brain regions¹⁰. In the presence of AD biomarkers, a pattern of hyper-connectivity has been observed in preclinical stages, followed by hypo-connectivity in subsequent stages,

mirroring tau's topographical spreading^{11–14}, starting with connectivity alterations between the tErC region and other regions of the MTL, as well as with its connected anterior and posterior cortical regions^{15,16}. Such connectivity alterations have been related with increased tau load in cognitively unimpaired older adults, and this pattern, in turn, is related to their memory performance¹⁵.

However, the biological processes underlying AD neuropathology start decades before the emergence of clinical symptoms leading to AD diagnosis, such as the typical AD-related episodic memory impairment^{17,18}, so that individuals at the preclinical stage 1 of AD remain mostly asymptomatic. In other words, AD pathology can exist in the brain of older persons without dementia or mild cognitive impairment.

This is where the quest to improve identification of early cognitive markers of AD takes place, aiming to target sub-clinical cognitive changes specifically associated with preclinical AD neuropathology. This quest is challenged by the fact that the exact function of the tErC region in cognition is still unclear. Among the different roles attributed to the tErC region, it has

¹GIGA Research, CRC Human Imaging, University of Liège, Liège, Belgium. ²PsyNCog Research Unit, Faculty of Psychology, University of Liège, Liège, Belgium.

³CICPSI, Faculty of Psychology, University of Lisbon, Lisbon, Portugal. ⁴Proaction Laboratory, Faculty of Psychology and Educational Sciences, University of Coimbra, Coimbra, Portugal. ⁵CINEICC, Faculty of Psychology and Educational Sciences, University of Coimbra, Coimbra, Portugal.

 e-mail: emma.delhaye@uliege.be

been suggested that it is part of an anterior-temporal (AT) system of connected regions dedicated to object processing, which includes the perirhinal cortex, amygdala, inferior temporal and fusiform gyri, as well as lateral orbitofrontal and ventral temporopolar cortex. This system is distinct from a posterior-medial (PM) system dedicated to scenes and spatial processing, which involves the retrosplenial cortex, the thalamus, angular gyrus, precuneus, and posterior cingulate cortex (PCC)^{19,20}. Within the AT system, the tErC region is argued to support the viewpoint invariant, entity-level, representation of unique objects (i.e. a unique conjunction of perceptuo-conceptual features^{19,21,22}). In this framework, the respective scenes- and objects- systems should be involved in their dedicated level of information processing and representation, regardless of the cognitive function involved (e.g. be it episodic memory or perception²¹). Based on this idea, we proposed that entity representation should be specifically affected by changes to the integrity of the tErC, regardless of the function recruited (episodic memory, semantic memory, perception), thereby representing a potential cognitive marker of the preclinical stage of AD^{23–25}.

Indeed, structural integrity of the tErC region has been shown to predict performance in older adults on the continuum of AD in a series of cognitive tasks hypothetically involving entity-level representation (for a review, see ref. 24), such as viewpoint invariant fine-grained perceptual discrimination of objects with overlapping features²⁶, intra-item configural processing²⁷, familiarity-based memory^{28,29}, familiarity for unique entities²⁵, memory for unisited representations^{30,31}, fine-grained object mnemonic discrimination^{32,33}, fine-grained object conceptual knowledge³⁴, fine-grained object conceptual discrimination³² and naming of confusable objects³⁵. In the same vein, decreased fine-grained object mnemonic discrimination was associated with hypoactivity in the tErC region^{36–38} and tErC-hippocampus activity functional imbalance³⁸. Another study showed that decreased fine-grained object mnemonic discrimination in low-performing older adults is related to resting-state functional hyperconnectivity between the tErC region and CA3 of the hippocampus, in relation with increased A β pathology³⁹. Tau levels were also shown to be associated with worse fine-grained object mnemonic discrimination in healthy older adults^{37,40}. Finally, behavioural evidence of impaired performance in tasks known to involve the tErC, like complex object visual discrimination^{41–44}, short-term conjunctive binding (see ref. 45 for a review), or fine-grained object naming⁴⁶, distinguishes between healthy and ‘at-risk’ older individuals or individuals in early stages of AD.

Yet, these results all come from different populations, methodologies, and labs. A necessary step would be to assess the relationship between the integrity of the tErC and a series of tasks involving entity-level representation in a single population, which only few studies have done until now^{26,32}. Here, we aimed at testing multiple functions involving entity-level representation, such as fine-grained perceptual discrimination and fine-grained mnemonic discrimination (versus these same functions but involving scene representations), to test the hypothesis that the tErC region should be involved in all tasks requiring that specific type of representation, irrespective of the process recruited. Consequently, we expect tErC alterations to be associated with impaired performance across all tasks involving entity representations, but not scene representations. Moreover, the novelty of this study is that we included a measure of objects and scenes visual similarity when assessing discrimination, as a proxy of the granularity of the discriminative process engaged³².

We assessed fine-grained perceptual discrimination (with an odd-one-out task, i.e. gold standard in the literature, used in a variety of studies measuring fine-grained perceptual discrimination^{47–49}) and mnemonic discrimination (with recognition memory) in 51 nominally healthy older adults. In this study, we adopted a correlational approach and targeted a participant group with a broad distribution of cognitive abilities and MTL integrity. This was based on the considerations that 5 to 10% of cognitively unimpaired older adults are actually in a preclinical stage of AD, exhibiting neocortical tau pathology despite the absence of cognitive symptoms^{50,51}, that tau accumulation in the tErC is associated with regional volume loss⁷, and that the presence of mild cognitive impairment, as detected by the

MoCA, is linked to tErC volume reduction⁵². We related each participant’s sensitivity to visual similarity to the volume and resting-state functional connectivity of their MTL regions. Because Deep Convolutional Neural Network (CNN) has proved increasingly successful in mapping brain visual representations^{53,54}, we characterised visual similarity between objects vs. scenes pictures using the AlexNet CNN⁵⁵, following previous methodologies^{53,54,56}. CNNs are composed of multiple layers, and as these layers progress, their nodes become sensitive to increasingly more complex, higher-level visual image features, similarly to what is described along the human ventral visual pathway. Here, we computed an index of sensitivity to visual similarity by correlating each participant’s trial-by-trial accuracy with trial-by-trial CNN-based visual similarity measures, following previous studies^{32,57}. We also replicated this method using human subjective ratings of visual similarity.

The overall aim of the study was to relate early tErC structural and/or functional alterations with a series of refined behavioural measures, towards improving early clinical detection of AD pathology. This, in turn, contributes to informing and refining models of the role of MTL subregions in cognition. Results showed a specific relationship between participants’ sensitivity to visual similarity and their tErC structural integrity (and BA36 in the memory task) for object discrimination and their postero-medial entorhinal cortex (pmErC) integrity for scene discrimination. The relationship with the tErC integrity was, however, dependent on the measure of visual similarity used to compute the indices of sensitivity, with fine-grained perceptual discrimination associated with objective measures of intrinsic featural similarity, while fine-grained mnemonic discrimination was associated with subjective human ratings. In addition, although perceptual discrimination was associated with an unspecific pattern of resting-state functional connectivity, regardless of the visual similarity measure, and while non-specific patterns were also found using an objective measure from a CNN in relation with mnemonic discrimination, using a subjective measure of similarity led to specific associations between the integrity of the connectivity between the tErC and BA36 for objects, and between the pmErC and CA1 and the parahippocampal cortex (PhC) for scenes.

Results

Fine-grained perceptual discrimination was assessed using an odd-one-out task, and subsequent fine-grained mnemonic discrimination was assessed in a yes-no recognition test based on the items presented in the odd-one-out task. The design is illustrated in Fig. 1.

Regions of the MTL, including hippocampal subfields, ErC, BA35 and BA36 in the left and right hemispheres, were automatically segmented with the Automatic Segmentation of Hippocampal Subfields toolbox⁵⁸. In addition, the ErC was subsequently manually segmented into its postero-medial and antero-lateral parts following established protocol from previous studies⁵². Intra-rater reliability measures regarding the manual segmentation of alErC and pmErC were excellent (left alErC: ICC = 0.976, mean Dice = 0.98 (SD = 0.01); right alErC: ICC = 0.992, mean Dice = 0.98 (SD = 0.01)) and comparable to previous studies^{25,52,59}. See Fig. 2 for an illustration of the result of the automatic and manual segmentation.

Behavioural performance was well above chance in all tasks (proportion of correct responses in the discrimination task, $M_{\text{object}} = 0.84$ (SD = 0.07), $t(49) = 76.86$, $p < 0.001$, Cohen’s $d = 10.87$; $M_{\text{scene}} = 0.87$ (SD = 0.06), $t(50) = 101.69$, $p < 0.001$, Cohen’s $d = 14.24$; Hits-False alarms in the recognition memory task, $M_{\text{object}} = 0.26$ (SD = 0.14), $t(46) = 12.30$, $p < 0.001$, Cohen’s $d = 1.79$; $M_{\text{scene}} = 0.48$ (SD = 0.14), $t(49) = 24.81$, $p < 0.001$, Cohen’s $d = 3.51$).

Behavioural analyses

The data plots are presented in Fig. 3. In the odd-one-out task, the GLMM indicated no main effect of condition (object or scene), $\chi^2 = 0.19$, $df = 1$, $p = 0.66$, but a main effect of visual distance, $\chi^2 = 30.87$, $df = 1$, $p < 0.001$, according to which accuracy increased with increased visual distance, and a significant interaction between condition and visual distance, $\chi^2 = 17.18$, $df = 1$, $p < 0.001$. The estimated marginal mean of linear trend for visual

Fig. 1 | Illustration of objects and scenes conditions in the odd-one-out and in the recognition memory tasks. Illustration of objects and scenes trials in the odd-one-out ($N = 48$ trials per condition) and in the recognition memory ($N = 48$ old and $N = 48$ new items per condition) tasks. In the odd-one-out, participants were instructed to identify the item that represented a different exemplar than the other two, which represented the same exemplar, seen from two different viewpoints. Object and scene conditions were blocked, and each odd-one-out task was followed by a 4-min break filled with mental calculation, and then a yes-no recognition memory test. Stimuli illustrated belong to databases from^{77,81}.

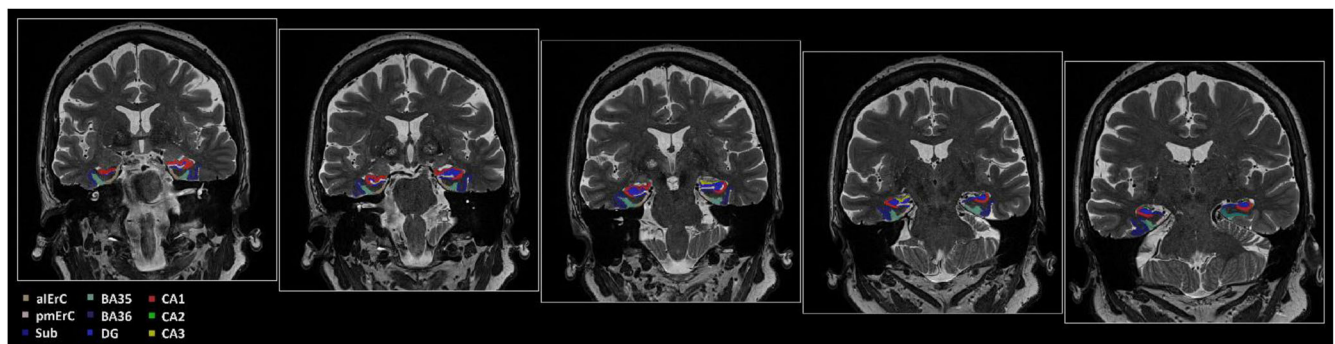
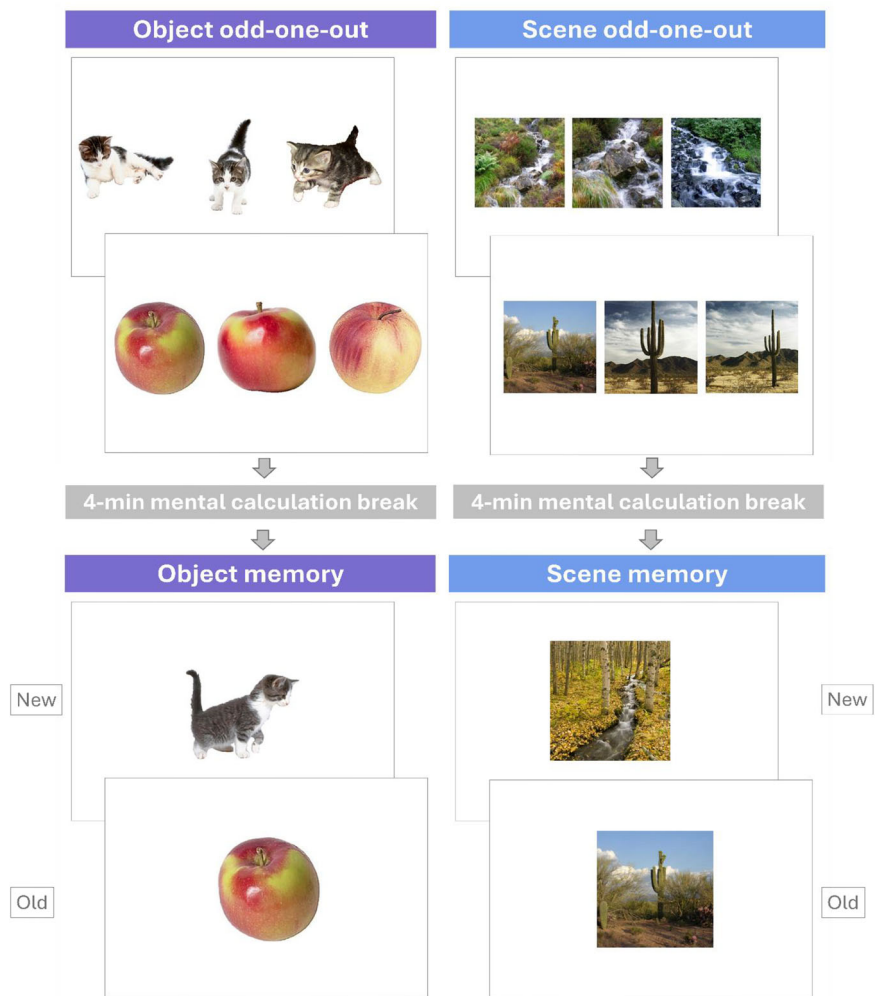


Fig. 2 | Result of the automated and manual segmentation of subregions in the MTL. Segmentation results are presented from anterior to posterior MTL. aErC anterior-lateral entorhinal cortex, BA35 Brodmann area 35, pmErC posterior-medial

entorhinal cortex, BA36 Brodmann area 36, PhC parahippocampal cortex, Sub subiculum, CA cornu ammonis, DG dentate gyrus.

distance was positive for objects (0.32) but not for scenes (-0.05), meaning that discrimination accuracy significantly increased as visual distance increased for objects, but the effect was not significant for scenes. The same analysis using the measure of visual distance judged by human raters showed a similar pattern of results, with, in addition, a main effect of condition according to which scenes are better discriminated than objects (see Supplementary Results and Supplementary Fig. 4).

In the recognition memory task, not taking visual distance into account in the analysis on the hits (i.e. correct recognition of targets; as the targets always had a 0 visual distance with themselves), paired samples t -tests

showed no significant difference in hit rates between objects and scenes, $t(46) = 1.79$, $p = 0.08$, Cohen's $d = 0.26$. However, the Hits-False alarms mnemonic discrimination measure revealed a significant difference between objects and scenes, $t(46) = 10.78$, $p < 0.001$, Cohen's $d = 1.57$, with scenes yielding better performance than objects. The GLMM on correct rejections indicated a main effect of condition (object or scene), $\chi^2 = 172.82$, $df = 1$, $p < 0.001$, with greater correct rejections of lures for scenes than objects ($M_{\text{object}} = 0.46$; $M_{\text{scene}} = 0.74$), a main effect of visual distance, $\chi^2 = 52.36$, $df = 1$, $p < 0.001$, according to which correct rejections increased with increased visual distance between the lure and its matched target, and a

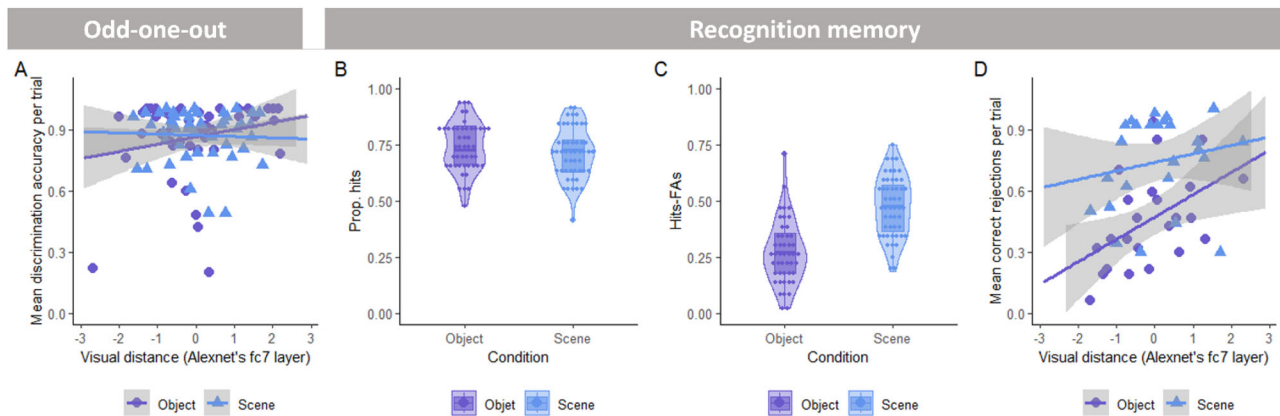


Fig. 3 | Plot of behavioural data for object and scene conditions across the odd-one-out and recognition memory tasks. **A** Discrimination accuracy in the odd-one-out task as a function of visual distance (centred-scale). Standard error is represented. Each dot represents a trial's mean accuracy across subjects; **B** Proportion of correct recognitions (Hits) for object and scene conditions in the recognition memory task. Box plot centre line, median; box limits, upper and lower quartiles; whiskers, 1.5x interquartile range; **C** Discrimination performance (Hits-

False Alarms (FAs)) for object and scene conditions in the recognition memory task. Box plot centre line, median; box limits, upper and lower quartiles; whiskers, 1.5x interquartile range; and **D** Correct rejections of lures for object and scene conditions as a function of the visual distance (centred-scale) to their matched targets. Standard error is represented. Each dot represents a trial's mean correct rejections across subjects. $N = 50$ subjects in the objects odd-one-out task, $N = 51$ in the scenes odd-one-out task, $N = 47$ for objects memory, and $N = 50$ for scenes memory.

significant interaction between condition and visual distance, $\chi^2 = 6.55$, $df = 1$, $p = 0.01$. The estimated marginal mean of linear trend for visual distance was positive for both objects (0.47) and scenes (0.23), suggesting that correct rejections increased as visual distance increased for both objects and scenes, but the effect was greater for objects. This interaction disappeared when using the measure of visual distance judged by human raters in the analyses, while the main effects remained (see Supplementary Results and Supplementary Fig. 5).

Relation with structural integrity

The relationship between MTL structures integrity and the impact of visual distance on performance was explored using an « accuracy sensitivity to visual similarity » measure, computed for each subject by correlating accuracy in each trial with the trial's index of visual distance, and then transforming each r -value into a Z-score with the Fisher transformation. These scores were computed separately for objects and scenes, and separately for each task (accuracy in the odd-one-out task, and lures discrimination accuracy in the recognition memory task). The participant's resulting « sensitivity to visual similarity » indices were then related to MTL structures integrity (volumes) using forward stepwise linear regressions with 12 regions of interest (ROI): left and right CA1, CA3, pmErC, BA36, tErC, and PhC.

In the odd-one-out task, results on the relation between sensitivity to visual similarity and the volumes of the different brain regions within the MTL revealed that the best model to explain the variability in the data included exclusively the bilateral tErC for objects ($F(2, 47) = 6.31$; $p < 0.01$; $R^2 = 0.21$), and exclusively the left pmErC for scenes ($F(1, 49) = 4.35$; $p = 0.042$; $R^2 = 0.08$). These effects disappeared when using a subjective measure of visual distance to compute the sensitivity to visual similarity, so that no region significantly predicted the variability in the data.

In the recognition memory task, for objects, results on the relation between sensitivity to visual similarity for lure identification and the volumes of the MTL sub-regions did not reveal any region to significantly explain the variability in the data. For scenes, the best model to explain the variability in the data included exclusively the left pmErC ($F(1, 48) = 8.73$; $p < 0.01$; $R^2 = 0.15$). Of note, we replicated the analyses from the recognition memory task while regressing out the variability due to sensitivity to visual similarity during perceptual discrimination, based on Gellersen et al.'s methods²⁶. The same pattern of results was the same, both for objects and for scenes. Moreover, computing the sensitivity to visual similarity index using subjective similarity ratings, the best model found to explain the variability

in the data included exclusively the right BA36 and right tErC for objects. We did not find evidence of any relation for scenes in this analysis (see Supplementary Results).

Relation with functional integrity

Seed-based connectivity. Relation between the four scores of sensitivity to visual similarity and the integrity of resting-state functional connectivity was first assessed through a seed-based connectivity analysis, relating the spatial pattern of functional connectivity across all voxels of the brain with a seed area while controlling for all other seeds. Seed regions included the 12 ROIs from the MTL (left and right CA1, CA3, pmErC, BA36, tErC, and PhC). Functional connectivity strength was represented by Fisher-transformed semi-partial correlation coefficients (ICC) (thus allowing controlling for any signal bleed between adjacent regions).

First, to characterise the pattern of connectivity, we computed the significant connectivity from all seeds to all voxels in relation with the sensitivity to visual similarity in each task. This result is illustrated in Fig. 4.

In the odd-one-out task, contrasting the resting-state connectivity patterns associated with objects' versus scenes' sensitivity to visual similarity resulted in a greater connectivity pattern between the right tErC and the left superior lateral occipital cortex for objects than scenes. The same contrast but using the index of sensitivity to visual similarity computed using subjective human ratings resulted in a greater connectivity between the right PhC and the right intracalcarine cortex for objects than scenes (see Supplementary Results).

In the recognition memory task, the objects versus scenes contrast between resting-state connectivity patterns associated with the index of sensitivity to visual similarity computed with AlexNet's fc7 did not lead to any significant difference. The same analysis using the sensitivity to visual similarity score computed using human subjective ratings resulted in greater connectivity between the right PhC and the right inferior lateral occipital cortex and the left middle frontal gyrus for objects than scenes.

ROI-to-ROI connectivity

A second analysis explored connectivity between selected ROIs belonging to the PM and the AT networks, respectively, both within the MTL and beyond i.e. for the AT system, we included: left and right tErC, BA36, superior frontal gyrus, orbito-frontal cortex, temporal pole, and medial prefrontal cortex; for the PM system: left and right pmErC, PhC, angular gyrus, superior and inferior lateral occipital cortex, precuneus, thalamus, and PCC.

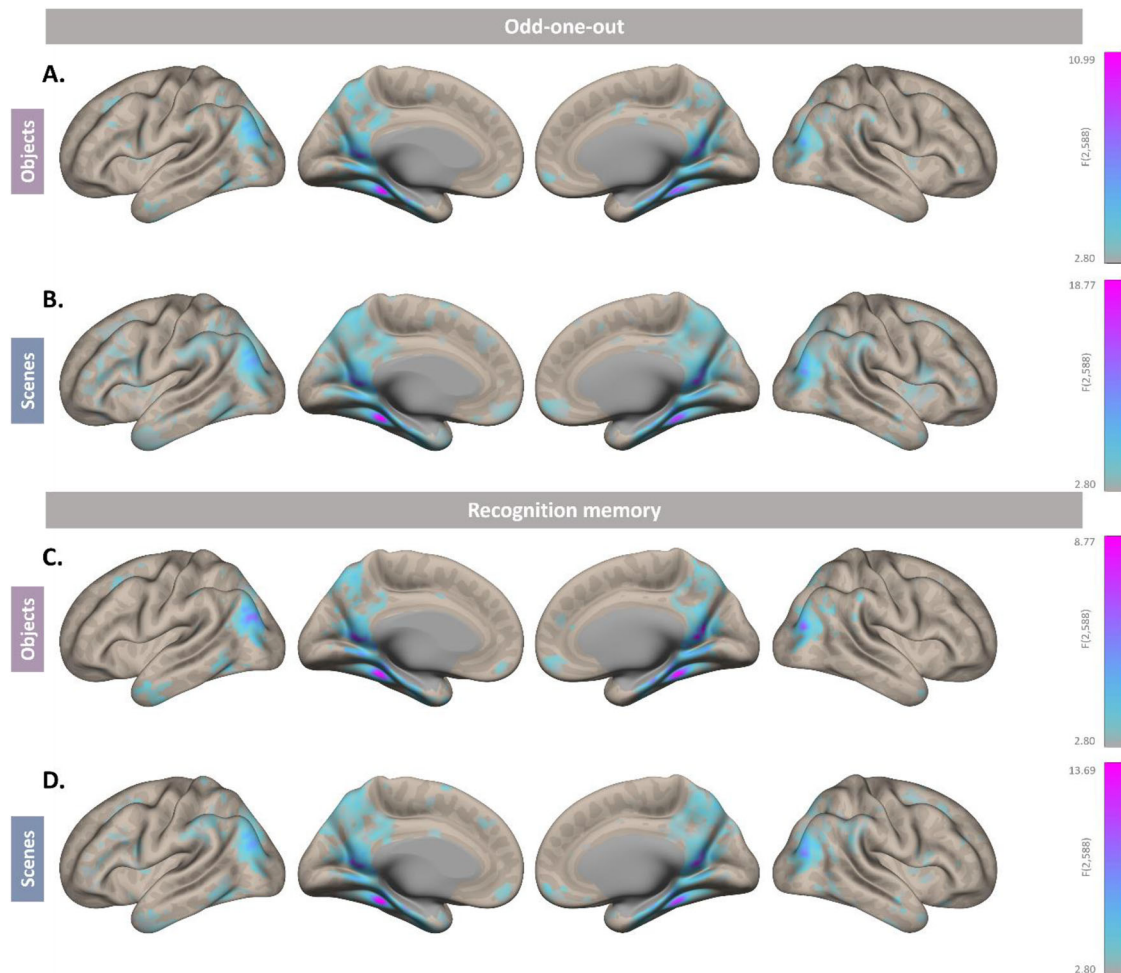


Fig. 4 | Seed-based connectivity patterns associated with indices of sensitivity to visual similarity in each task and each condition. Illustration of the seed-based connectivity patterns (Fisher-transformed semi-partial correlation values) associated with indices of sensitivity to visual similarity in each task (odd-one-out and recognition memory) and each condition (objects or scenes), from all seeds (selected ROIs from the median temporal lobe (MTL), i.e. left and right CA1, CA3, tErC (including anterior-lateral entorhinal cortex and BA35), pmErC, BA36, PhC).

A Seed-based connectivity pattern associated with sensitivity to visual similarity for objects in the odd-one-out task. **B** Seed-based connectivity patterns associated with sensitivity to visual similarity for scenes in the odd-one-out task. **C** Seed-based connectivity patterns associated with sensitivity to visual similarity for objects in the recognition memory task. **D** Seed-based connectivity patterns associated with sensitivity to visual similarity for scenes in the recognition memory task. $N = 51$ subjects.

We additionally included regions of the hippocampus: left and right CA1 and CA3. Functional connectivity strength was represented by Fisher-transformed semi-partial correlations, which allowed controlling for any signal bleed between adjacent regions.

First, we assessed the connectivity between all ROIs (29 in total, see Fig. 5), independently of task performance. Results showed extensive connectivity among regions from the MTL as well as between MTL regions and predefined ROIs from the PM and the AT systems, both between hemispheres and between PM and AT systems. Beyond the MTL, there were also connections between the PM and AT predefined ROIs. The bilateral tErC showed connections with BA36, the temporal pole, PhC, pmErC, CA1, and CA3. In addition to this connectivity pattern, MTL regions belonging to the PM system (bilateral pmErC and PhC) showed connections with predefined ROIs from both the PM and the AT system.

All connections are represented in Fig. 5.

Then, we used forward stepwise linear regression analyses to assess the association between the connections among selected ROIs (i.e. first-level connectivity strength values) and the indices of sensitivity to visual similarity, tested one at a time (4 indices in total, derived from object and scene conditions, for both odd-one-out and recognition memory tasks). To reduce the number of measures entered in the analysis, we ran separate analyses including exclusively regions from the AT system and the hippocampus on

one hand, and of the PM system and the hippocampus on the other hand. Additionally, we restricted the analyses to selected hypotheses-driven connections involving tErC connectivity and pmErC connectivity, respectively.

In the odd-one-out task, results on the relation between sensitivity to visual similarity and resting-state functional connectivity revealed that, for objects, within the AT system, the best model to explain the variability in the data included exclusively the connectivity between the left tErC and left CA3 ($F(1, 48) = 6.88$; $p < 0.05$; $R^2 = 0.12$), and within the PM system, the connectivity between the right and left pmErC ($F(1, 48) = 5.18$; $p < 0.05$; $R^2 = 0.10$). For scenes, within the AT system, the best model included exclusively the connectivity between the right tErC and the left CA1, left CA3 and right BA36 ($F(3, 47) = 5.62$; $p < 0.01$; $R^2 = 0.26$), while within the PM system, no model reached significance (see Table 1). When using a subjective measure of visual distance to compute the sensitivity to visual similarity index, all relationships disappeared for objects, while for scenes, the best models to explain the variability in the data included, in the AT system, the connectivity between the left tErC and left orbito-frontal cortex and in the PM system, the connectivity of the left pmErC with the right thalamus, the right CA3 and the right pmErC (see Supplementary Results and Table S1).

In the recognition memory task, results on the relation between sensitivity to visual similarity for lure identification and the resting-state

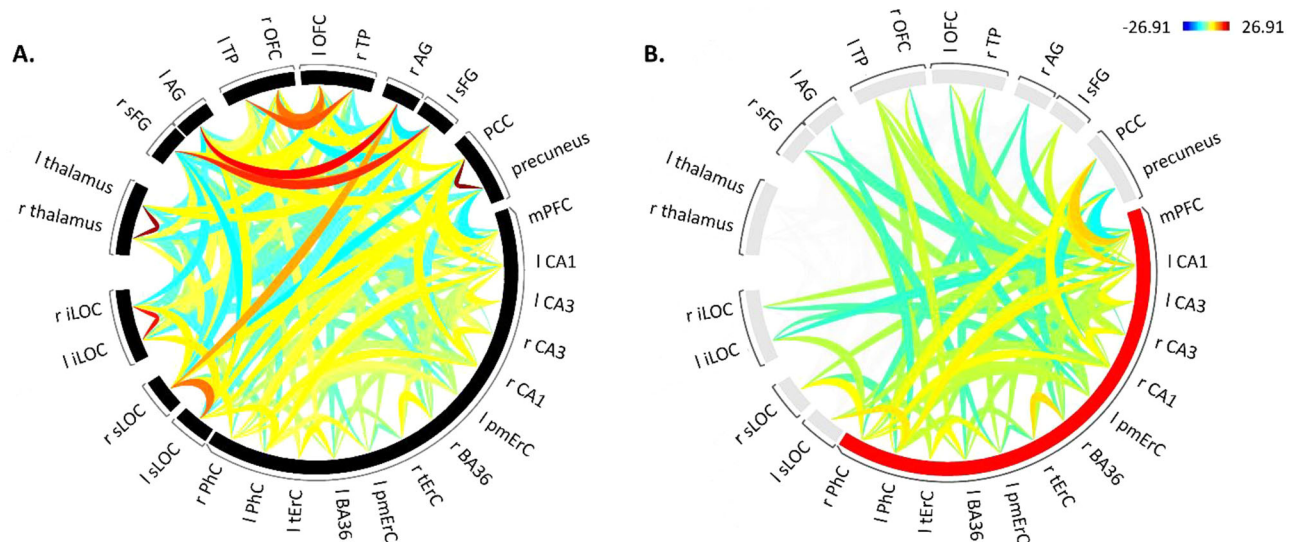


Fig. 5 | ROI-to-ROI connectivity patterns. Illustration of the ROI-to-ROI connectivity patterns (Fisher-transformed semi-partial correlation values), including selected ROIs from the medial temporal lobe (MTL) and ROIs from regions belonging to the postero-medial (PM) and antero-temporal (AT) systems as well as hippocampal subfields cornu ammonis (CA) 1 and CA3. **A** ROI-to-ROI connections between regions within and beyond the MTL belonging to the PM and AT systems, as well as hippocampal subfields CA1 and CA3. **B** Display centered on the

connectivity involving the MTL cluster (in red, with other ROIs in light grey). tErC transentorhinal cortex, including anterior-lateral entorhinal cortex and Brodman area (BA) 35, pmErC posterior-medial entorhinal cortex, BA36 Brodman area 36, PhC parahippocampal cortex, CA cornu ammonis, TP temporal pole, AG angular gyrus, OFC orbito-frontal cortex, SFG superior frontal gyrus, mPFC median pre-frontal cortex, iLOC inferior lateral occipital cortex, sLOC superior lateral occipital cortex, PCC posterior cingulate cortex. $N = 51$ subjects.

connectivity of the different regions did not reveal any connectivity pattern to significantly explain the variability in the data, neither for objects nor for scenes, in the AT system. However, in the PM system, there was a significant model for scenes, with connectivity of the right pmErC with the right CA1, left superior lateral occipital cortex, and left thalamus ($F(3, 46) = 6.92$; $p < 0.001$; $R^2 = 0.31$) (see Table 1). When using a subjective measure of visual distance to compute the sensitivity to visual similarity index for object lure identification, the best model included the connectivity between the right tErC and left BA36 in the AT system, but no model reached significance in the PM system. For scenes, no model reached significance in the AT system, but in the PM system, the best model to explain the variability in the data included the connectivity of the left pmErC with the left CA1, and of the right pmErC with the left PhC (see Supplementary Results and Table S1).

Discussion

This study aimed to test the hypothesis that the tErC is central to fine-grained entity-level, viewpoint invariant, representation and is involved in all cognitive functions recruiting that level of representation, and that, as such, and as the tErC stands among the first regions to be affected by AD neuropathology, consistent impairment in entity-level representation across multiple cognitive functions should provide a sensitive marker of tErC alteration²⁴. Because the presence of AD neuropathology in the tErC has been associated with a loss of both structural^{13,5–8,60} and resting-state functional^{11,60} integrity in this region, we analysed tErC volumes and resting-state connectivity patterns, in relation with performance in two tasks that recruited entity-level representations: fine-grained perceptual and fine-grained mnemonic object discrimination. Scene discrimination was also tested to ensure the specificity of the relation. To characterise the demand on fine-grained discrimination, we used a novel metric that captures the extent to which accuracy is affected by visual similarity between similar objects/scenes, calculated using visual similarity measures from the AlexNet CNN⁵⁵.

Our results revealed lower memory discrimination for objects than scenes, in line with existing studies showing a decline in object, but not scene, mnemonic discrimination in aging^{36,40}. But importantly, the novelty of our study is to show that this effect on objects is mitigated by the visual similarity

of the to-be-discriminated items, and thus, by the demands on the discrimination processes: the more similar the objects are, the more performance is impacted. This means that testing discrimination between items representing a same concept is not enough to provide a sensitive measure of discrimination; visual similarity should be taken into account. This was especially the case for objects, while scene discrimination was affected by visual similarity to a lesser extent.

The main outcome of this study is evidence for a specific marker of tErC structural integrity, through the measure of sensitivity to visual similarity for object perceptual discrimination. Our results indeed showed a relation between tErC structural integrity and sensitivity to visual similarity, such that the more participants' performance is affected by visual similarity in object perceptual discrimination, the smaller their tErC. This is well in line with previous results showing an involvement of the tErC in object perceptual discrimination²², and a relation between object perceptual discrimination and the integrity of this region²⁶. Yet, our hypothesis that this relation should be visible regardless of the cognitive function involved, as long as it recruits entity-level representation, was not directly confirmed, as we did not observe any such relation in the object recognition memory task, despite extensive evidence in the literature showing an involvement of the tErC in object memory (for review, see ref. 23) as well as an impairment of object memory in association with tErC alteration in aging and in the continuum of AD (for a review, see ref. 24). However, though, in support of the idea of a regional representational specificity, our supplementary analyses showed that while the CNN objective measure of visual similarity did not capture the impact of visual similarity on memory performance for objects in relation with tErC integrity, there was a relation between tErC and BA36 integrity and sensitivity to visual similarity computed using subjective independent human ratings. Although this result was not expected, it makes sense, as one could interpret that tErC-based fine-grained discrimination might be sensitive to different similarity measures depending on the nature of the task: objective measures of intrinsic featural similarity could be representative of the information used when doing perceptual discrimination, but might not fully capture the similarity between the lure and the stored memory representations, which might, in turn, be better captured by subjective human ratings. The distinction between objective measures of visual similarity and subjectively-rated similarities might be worth exploring

Table 1 | Summary of the significant associations identified through stepwise regressions on seed-based functional connectivity measures between regions of interest (ROIs) within the AT and PM networks

	Odd-one-out				Recognition memory			
	Objects		Scenes		Objects		Scenes	
	Best model	R^2	Best model	R^2	Best model	R^2	Best model	R^2
AT network	l tErC - l CA3 *	0.12	r tErC - l CA1 * r tErC - l CA3 ** r tErC - r BA36 *	0.26	-	0.0	-	0.0
PM network	l pmErC - r pmErC *	0.10	-	0.0	-	0.0	r pmErC - r CA1 *** r pmErC - l sLOC * r pmErC - l Thalamus *	0.31

These associations were examined in relation to perceptual and mnemonic discrimination sensitivity to visual similarity for objects and for scenes, using visual similarity computed from the fc7 layer of AlexNet. AT network includes left (l) and right (r) tErC, BA36, superior frontal gyrus (SFG), orbito-frontal cortex (OFC), temporal pole (TP), CA1, CA3, and medial prefrontal cortex (mPFC). PM network includes left (l) and right (r) pmErC, PhC, angular gyrus (AG), superior (sLOC) and inferior lateral occipital cortex, precuneus, thalamus, CA1, CA3, and PCC. * $p < 0.05$, ** $p < 0.01$, *** $p < 0.001$. $N = 51$ subjects.

in the future, as the tErC has recently been shown to precisely track the observer-specific perceived visual similarity among category exemplars in an fMRI study⁶¹.

Moreover, our results outlined that the integrity of the left pmErC is specifically associated with the sensitivity to visual similarity for scenes, both for perceptual and mnemonic discrimination. This result is also well in line with the existing literature acknowledging a role of the pmErC in spatial information and spatial context processing, and brings further support to it^{62,63}.

In terms of resting-state functional integrity measures, in regards to cognition, one previous study had shown a specific relationship between resting-state tErC-CA3 functional connectivity and memory scores in low performers of an object mnemonic discrimination task, connectivity which in turn was related with the presence of AD neuropathology and ErC volume loss³⁹. Although the current study showed a similar relation between tErC-CA3 functional connectivity and sensitivity to visual similarity in object perceptual discrimination, it was not specific, since evidence of this relationship also existed for scene perceptual discrimination. In the same vein, relationships were shown between connectivity of the pmErC with the PM system and with the hippocampus and sensitivity to visual similarity for object perceptual discrimination, rendering the results from object perceptual discrimination quite unspecific. These relationships remained unspecific regardless of the measure of visual similarity used to compute the scores in the ROI-to-ROI analysis. The seed-based analysis contrasting objects versus scenes-related significant connectivity patterns, however, complemented the picture by showing greater tErC-sLOC connectivity for objects than for scenes.

Several reasons could contribute to the lack of specificity in the resting-state connectivity results, notably concerning the relation shown of the AT system in scene perceptual (but not mnemonic) discrimination. Notably, it could be the case that scenes were processed like items in that task, as they were presented as pictures side by side; yet this is not supported by the results of volumetric regressions that showed evidence of a very scene-specific region associated with scene discrimination. Another interpretation is that scenes are composed of series of unique items that are processed by the object-dedicated system, and those items might have been diagnostic and thus key to discriminate between similar scenes.

However, consistently with structural results, although resting-state connectivity patterns associated with object recognition memory did not show relationships between the tErC and other regions of the AT system when using an objective measure of visual similarity, it did so when using a subjective measure of visual similarity. In that case, there was a significant and specific contribution of the connectivity between the tErC and BA36 to object memory, closely mirroring results from structural integrity analyses, while no relationship was significant for scenes in the AT system. In turn, relationships involving the connectivity of the pmErC with the PM system and the hippocampus were evidenced for scenes, but not object, mnemonic discrimination, irrespective of the measure used to compute visual similarity. This supports the idea proposed earlier that objective measures might

not be fully representative of the similarity between the lure and the stored memory representation, and that subjective measures might be better suited to tackle similarity in that case.

Although the results from the perceptual discrimination task are unexpectedly unspecific, these results from mnemonic discrimination are well in line with the literature, supporting the view according to which the AT system is involved in object processing while the PM system is dedicated to scene processing¹⁹. The specific relationship between tErC-BA36 connectivity and object mnemonic discrimination is particularly interesting as BA36 is directly neighbouring the tErC as part of the perirhinal cortex. Yet, it is the first time, to our knowledge, that such relationship is shown using resting-state connectivity, and it will need to be replicated in future studies. More generally, the respective roles of the tErC and BA36 critically need to be further explored, as it is not the first time that the structural integrity of BA36 is shown to be associated with object memory in older adults, in a fashion that is sensitive to similarity (e.g. ref. 32).

Authors have argued that functional connectivity alterations might precede structural damage in the propagation of AD neuropathology⁶⁰. While the current study does not exclude this idea and shows some support to it, it still seems that the relation of such early connectivity dysfunction with cognition is subtle to isolate specifically, as our analyses on perceptual discrimination did not show any specificity in the relationships. The relationship between targeted cognitive measures and functional connectivity will need to be further explored and better understood in future studies.

While we argue that it is critical to take into account objects visual similarity when assessing discrimination, as a measure of the granularity of the discriminative process engaged, and while we think it makes sense to do so, especially when targeting discrimination between similar entities representing a same concept, the tErC region has also been involved in fine-grained conceptual discrimination⁶⁴, which was not directly represented here. CNN measures indeed do not carry semantic information per se, and this was shown to be a limiting factor in their ability to map the activity of the higher visual brain regions, including the tErC^{54,65}. In addition, sensitivity to conceptual similarity has been shown to be related with perirhinal cortex (BA36) structural alterations in healthy aging and AD³². Future studies should integrate semantic similarity measures on top of visual similarities computed using CNNs, to better target the sensitivity to similarity of the tErC.

We also reckon that a forced-choice recognition memory task might have been more suited to target memory discrimination instead of a yes-no paradigm⁶⁶, as impairments in yes-no recognition tasks might partially reflect executive, rather than mnemonic, dysfunction²⁶. In addition, the yes-no recognition task used here does not preclude hippocampal contribution to memory performance, contrary to speeded tasks thought to prevent slower hippocampal contributions, and thus, to better isolate the function of the tErC⁶⁷. However, our results remain in line with other studies that have reported a tErC involvement in memory while using a yes-no recognition paradigm³⁹, so the test format should not be seen as a definite limiting factor.

Table 2 | Participants demographics

	Mean (SD) [range]
Male/Female	20/31
Age	69.49 (3.65) [65–83]
Education	14.59 (3.44) [6–24]
MoCA (/30)	27.75 (1.83) [22–30]
ECog	56.42 (11.40) [39–86]

Another limitation is that the tErC, located within the MTL, is particularly prone to signal distortion and loss in fMRI due to its proximity to the sinuses⁶⁸. While we applied post-processing precautions to mitigate this issue, future studies should address this challenge at the acquisition stage by implementing sequences specifically designed to enhance the signal-to-noise ratio in these regions^{69,70}.

Finally, although the current findings provide theoretical insights into the role of the tErC and the identification of its structural and functional alterations, future studies should replicate this task while including biomarkers of AD pathology. This would help establish the AD-specificity of the observed relationships and improve the translational relevance of these results for clinical applications in AD.

Conclusion

This study tested the hypothesis that the tErC region, which stands among the first regions affected by AD neuropathology, supports the fine-grained representation of individual object entities. As such, any cognitive function involving entity representation should be impaired compared to scene representation in the presence of early AD neuropathology in the tErC, and it should be increasingly the case with the increased demands on the discriminative process engaged. We showed the expected behavioural pattern of results, with participants' sensitivity to visual similarity being specifically related to their tErC structural integrity for object discrimination (and BA36 in the memory task), and to the integrity of the left pmErC for scenes discrimination. In addition, the only specific relationship shown between tErC resting-state functional integrity and the sensitivity to visual similarity indices emerged with the left BA36, in relation with object mnemonic discrimination, while scene mnemonic discrimination involved a larger connectivity network between the pmErC and other regions of the hippocampus and PM system. The relationship with the tErC integrity was however dependent on the measure of visual similarity used to compute the indices of sensitivity, so it might be the case that different measures of similarity (objective or subjective ratings) are representative of the demands on the discriminative processes engaged in the tErC depending on the nature of the task, mnemonic or perceptual. Taken together, these findings suggest that discrimination sensitivity to object visual similarity may serve as a specific marker of tErC structural integrity after accounting for the type of similarity measured, although we could only find specific relationships in the memory task for its functional integrity.

Methods

Participants

A total of 51 participants took part in the study. Participants were community-dwelling, nominally healthy, older adults, between 65 and 83 years old, with no neurologic or psychiatric history, no MRI contraindication, and normal or corrected-to-normal vision. Participants' high-level visual abilities were screened using the Overlapping Figures Task of the Birmingham Object Recognition Battery (BORB)⁷¹, which did not lead to the exclusion of any participant. Cognitive status was assessed using the Montreal Cognitive Assessment (MoCA)⁷², but no participant was excluded on that basis, as we aimed for a participant group with a good distribution of cognitive abilities and MTL integrity, following previous studies⁵⁹ and as the presence of mild cognitive impairment detected through the MoCA is associated with tErC volume loss⁵². Every day, cognitive functioning was characterised using the ECoG questionnaire⁷³. The study was approved by the Ethics Committee of

the Liège University Hospital, and participants signed an informed consent before taking part to the experiment. Participants' demographic information is presented in Table 2.

Data from one participant was discarded in the odd-one-out task for objects, from four participants in the memory task for objects, and from one participant in the memory task for scenes, due to misunderstanding of the task instructions or pressing a wrong response key. Therefore, the final sample was of 50 subjects in the odd-one-out task for objects, 51 in the odd-one-out task for scenes, 47 for object memory, and 50 for scene memory.

Materials

Odd-one-out task. Forty-eight triplets of object pictures and 48 triplets of scene pictures were selected from existing databases (objects^{74–80}; scenes^{81–83}). In each triplet, two pictures represented the same object or the same scene, but from different viewpoints, and the third picture represented another exemplar of the same concept of object or scene.

Recognition memory. We selected one picture from each of the 48 triplets of the previous phase for each condition, object or scene (16 of them were the targets, viewpoint 1, 16 were the targets, viewpoint 2, and 16 were the 'odd' ones). We then matched each of these pictures with a new picture, i.e. the lure, representing another exemplar of the same concept. This resulted in 48 new object pictures and 48 new scene pictures. This task and the odd-one-out task are illustrated in Fig. 1.

Visual similarity measures. We assessed the complex visual properties of our image sets by evaluating the similarity of visual features derived from the pre-trained CNN AlexNet. AlexNet was trained on 1.2 million high-resolution images, categorising them into 1000 distinct categories (or classes). AlexNet consists of eight layers, including five convolutional layers (conv1 - conv5) and three fully connected layers (fc6 - fc8). Each convolutional layer takes input from the previous layer, using filters sensitive to different types of visual input⁸⁴. By construction, the filters of the first convolutional layers capture low-level properties of stimuli, such as edges with specific spatial frequencies and orientations, as well as colour information⁸⁵, while the later layers detect more complex visual features, such as the presence of specific visual objects or object parts (e.g. dog legs, bird eyes), across various spatial scale and viewing angles⁸⁵. To obtain the activation values from the CNN for our set of images, we presented each image (objects and scenes separately) to the pre-trained network, which generated activation values for each node in each layer for each image.

To reduce the number of measures analysed and because consecutive layers are highly correlated, we extracted the activation values for three representative layers for each image (layers conv3, fc6 and fc7, corresponding to early, middle, and late layers, respectively). For each of these layers, we compared the activation values of each image against all other images in the dataset (objects and scenes separately, $N = 192$ images per set) using Euclidian distance, producing a similarity matrix for each layer.

For the odd-one-out task, we extracted the Euclidean distance between the value of the 'odd' image in each triplet and its two associated target images for each representative layer. The average of these two distances was used to compute a single value of visual distance per triplet. For the recognition memory task, we extracted the Euclidean distance between the target image and its corresponding lure.

Here, we present data analysed using the late visual layer (fc7); information and analyses on other layers (conv3 and fc6), as well as from human subjective ratings of visual distance acquired through a pilot study, can be found in the Supplementary Methods and Supplementary Results.

Procedure

Data collection took place at the research centre, in a dedicated testing room. The experimenter explained task instructions and then left the room during the completion of the tasks by the participants, who did so on a laptop. The experimenter remained available in the next room to answer questions, if any. This study was part of a longer protocol that included other tasks, so

participants had to come twice to the lab. For this study, the total acquisition duration was of about 2 h.

Odd-one-out task. Object and scene tasks were built using PsychoPy⁸⁶. For each trial, the three pictures of a triplet were presented side by side on the screen. The order of trials was randomised across participants. Participants were instructed to identify the item that represented a different exemplar than the other two items, using the left, down and right arrow keys, depending on the item's position on the screen (left-side, middle, or right-side of the screen, respectively). Each trial ended with the participant's keypress or, in the absence of such, lasted a maximum of 10 s. An absence of response was treated as an incorrect response. This was followed by a 500 ms blank screen and a 500 ms fixation cross before the start of the next trial. Conditions for scenes and objects were presented in separate blocks. The subsequent memory test started only after the entire odd-one-out block (objects or scenes) was completed. Once the memory test for one condition was finished, participants proceeded to the odd-one-out task for the other condition, followed by its respective memory test. The order of object and scene conditions was counterbalanced across participants. The task is illustrated in Fig. 1.

Recognition memory. There was a 4-min break between the odd-one-out task and the start of the memory task (object or scene), filled with calculations. For the memory test, items were presented one by one on the screen (48 targets and 48 lures) in a pseudo-randomised order. Participants were instructed to determine, for each item, whether it had been seen in the previous task or not, answering with the « a » and « p » keys. Each trial ended with participants' keypress, or in the absence of such, lasted a maximum of 6 s, and was followed by a 500 ms blank screen and a 500 ms fixation cross, before the start of the next trial.

MRI acquisitions

Images were acquired on a 3 T Siemens Prisma scanner with a 64-channel head coil. Two anatomical images were acquired: a T1-weighted structural MRI (acquisition matrix = $256 \times 240 \times 224$, voxel size = $1 \times 1 \times 1 \text{ mm}^3$) and a high-resolution T2-weighted structural MRI (acquisition matrix = $448 \times 448 \times 60$, voxel size = $0.4 \times 0.4 \times 1.2 \text{ mm}^3$) with a partial field of view covering the entire MTL with an oblique coronal orientation perpendicular to the long axis of the hippocampus. The quality of each image was systematically visually checked, especially the T2-MRI, which is highly sensitive to motion (after reminding the participant to stay still during the entire subsequent 8 min of acquisition), and re-run in case of poor quality due to excessive motion. When T2 images were acquired twice ($N = 7$), we selected the one with the best quality for further processing. In addition, multislice T2*-weighted, eyes open, resting-state functional images were acquired with the multi-band gradient-echo echo-planar imaging sequence (CMRR, University of Minnesota) using axial slice orientation and covering the whole brain (36 slices, multiband factor = 2, FoV = $216 \times 216 \text{ mm}^2$, voxel size $3 \times 3 \times 3 \text{ mm}^3$, 25% interslice gap, matrix size $72 \times 72 \times 36$, TR = 1.7 s, TE = 30 ms, FA = 90°). The three initial volumes were discarded to avoid T1 saturation effects.

Data preprocessing

All data were BIDSified using an automated pipeline⁸⁷.

MTL regions segmentation

High-resolution T2-weighted MRI images were labelled using the Automatic Segmentation of Hippocampal Subfields software package (with atlas package 'ashs_atlas_upennpmc_20161128' obtained from the NITRC repository made available on the ASHS website)⁵⁸. The hippocampal subfields, the ErC, BA35 and BA36 in the left and right hemispheres were thereby labelled in each participant. Each output from ASHS underwent visual quality control.

The ErC was further manually subdivided into alErC and pmErC, following established protocols from previous studies (e.g. refs. 25,52). Intra-

rater reliability was assessed by separately comparing the segmentation of the right and left alErC of five randomly selected scans, completed by the same rater (ED) after a delay of 6–8 months. Consistency between measurements was evaluated using intraclass ICC using the type (3, B) to compute intra-rater consistency⁸⁸ and spatial overlap was assessed with the Dice metric (using the mean Dice value across the selected scans; Dice values are derived using the formula $2 * [\text{intersecting volume}] / [\text{original segmentation volume} + \text{repeat segmentation volume}]$). Both measures fall between 0 and 1, with higher values indicating greater reliability. Figure 2 illustrates the results of the segmentation, both automated and manual, for the al- and pm-ErC of the MTL.

For all subregions belonging to ErC and perirhinal cortex (BA35 and BA36), volumes were normalised by the extent of their segmentation in the slice direction (hippocampal axis), by dividing their volume by the product of the number of slices and the slice thickness⁵⁸. Additionally, all regional volumes were adjusted before analyses to account for total estimated intracranial volume (ICV) for each participant using the formula $\text{Volume}_{\text{adjusted}} = \text{Volume}_{\text{raw}} - \beta_{\text{ICV}}(\text{ICV}_{\text{indiv}} - \text{ICV}_{\text{mean}})$, where β refers to the regression coefficient of the model on a given regional volume of interest while using ICV as a predictor. This approach is based on extensive prior work (e.g. refs. 26,27,30).

The volume of our main region of interest, the tErC, was then computed as the sum of BA35 and alErC.

ROI definition. These MTL regions were additionally used as seeds and ROIs for resting-state connectivity analyses. To do so, left and right hemispheres atlases were coregistered to the subject's T1 space using the transformation matrix provided by ASHS and the flirt function of FSL⁸⁹. Similar to the volumetric analyses, BA35 and alErC regions were merged into one single tErC label using FSL.

To ensure that all ROIs had reliable signal despite the susceptibility artefact causing signal dropout in the MTL⁶⁸, we calculated the mean signal across the total grey matter and excluded voxels with signal < 25% of the mean grey matter signal for each participant³⁹.

In addition to the MTL ROIs (i.e. left and right CA1, CA3, pmErC, BA36, tErC and PhC), we also identified a set of predefined ROIs for the ROI-to-ROI analysis, based on the existing literature, which have shown strong connectivity with the MTL and belong to the PM-AT network. Specifically, within the AT system, these include the left and right superior frontal gyrus, orbito-frontal cortex, temporal pole, and medial prefrontal cortex. As part of the PM system, we included the left and right angular gyrus, superior and inferior lateral occipital cortex, precuneus, thalamus, and PCC (see in ref. 15). The ROIs were defined using the atlas provided by the CONN toolbox. Of note, the results from this analysis were similar when replicating the analysis using predefined ROIs from the atlas used by Berron et al.¹⁵, so here we only present analyses on ROIs extracted from the CONN atlas.

Functional MRI data preprocessing. MRI data preprocessing was conducted with SPM 12 (Wellcome Trust Center for Neuroimaging, London, UK). For each subject, EPI time series were corrected for motion and distortion using Realign and Unwarp⁹⁰, and coregistered to the corresponding structural image. The structural image was then segmented into grey and white matter using the 'unified segmentation' approach⁹¹. The warping parameters were subsequently applied separately to the functional and structural images to produce normalised images with isotropic voxel size of 2 mm for functional images and 1 mm for structural images. No spatial smoothing was performed to preserve the high resolution of the images and enable more accurate signal quantification within spatially adjacent subregions. Potential outlier scans were identified using ART⁹² as acquisitions with framewise displacement above 0.9 mm or global BOLD signal changes exceeding five standard deviations^{93,94}. A reference BOLD image was computed for each subject by averaging all scans, excluding outliers.

Denoising and further analyses were conducted using CONN toolbox, release 22.a^{95,96}. Functional data were denoised using a standard pipeline,

which involved regressing potential confounding effects including white matter timeseries (5 CompCor noise components), CSF timeseries (5 CompCor noise components), movements regressors (6 components), outlier scans (below 252 factors)⁹⁴, session effects and their first order derivatives (2 factors), and linear trends (2 factors) within each functional run. This was followed by bandpass frequency filtering of the BOLD timeseries⁹⁷ between 0.008 Hz and 0.09 Hz. CompCor^{98,99} noise components within white matter and CSF were estimated by computing the average BOLD signal as well as the largest principal components orthogonal to the BOLD average, and outlier scans within each subject's eroded segmentation masks. Considering the number of noise terms included in this denoising strategy, the effective degrees of freedom of the BOLD signal after denoising were estimated to range from 47 to 95.4 (average 92.6) across all subjects.

Statistical analyses

Behavioural analyses. Behavioural analyses were run on JASP¹⁰⁰ for *t*-tests comparisons (1) to chance level (i.e. 0; one-sided one sample *t*-tests) and (2) between objects and scenes conditions in the memory task (i.e. two-sided paired sample *t*-tests), as well as on RStudio version 2023.12.1¹⁰¹ for Generalised Linear Mixed Models (GLMM; see below) on a trial-by-trial basis to account for the accuracy binary outcome (0, 1) of the dependent variables. GLMMs were fit with the package lme4¹⁰². GLMMs were run in each task separately (odd-one-out and recognition memory), with condition (object or scene) as within-subject factor, visual distance computed from the highest layer of AlexNet (fc7) as continuous predictor, applying a centre-scale (i.e. the mean of the variable was subtracted from each data point, shifting the mean to 0), and participant's ID as random factor. Following these GLMMs, post-hoc pairwise comparisons were carried out on estimated marginal means for a given effect of interest, with Tukey's adjustments when there were multiplicity issues using the emmeans package¹⁰³ and the function lsmmeans from lsmeans package to deal with continuous factors. Estimated marginal means from the models are reported.

In the odd-one-out task, the dependent variable was accuracy on each discrimination trial. In the GLMMs for the recognition memory task, because we were interested in discrimination abilities with increasing visual distance between the target and its matched lure, behavioural analyses were run on accuracy for lures (i.e. correct rejections of lures as a function of their visual distance with the target). While each target and its matched lure were presented during the yes-no recognition task, we decided to focus this analysis on the lures that were presented before the target, to avoid effects of target repetition on subsequent lure discrimination. We additionally compared the mean correct recognition (hit) rates and discrimination indices (Hits minus False Alarms) between objects and scenes using paired sample *t*-tests (therefore, not including visual distance, as a target cannot be visually distant from itself).

Plots of the results were generated using the ggplot2 package¹⁰⁴.

Volumes regression analyses. To explore the relationship between MTL structures integrity and the impact of visual distance on performance, we computed measures of « accuracy sensitivity to visual similarity » for each subject, by relating accuracy in each trial with the trial's index of visual distance using Pearson correlations, and then transforming each *r*-value obtained for each participant by a Fisher transformation to give a Z-score. These correlations were computed separately for objects and scenes, and separately for each task (accuracy in the odd-one-out task, and lures discrimination accuracy in the recognition memory task). The participant's resulting « sensitivity to visual similarity » indices were then related to MTL structures integrity (volumes) using linear regressions with the forward stepwise method (allowing to avoid issues of multicollinearity between measures) in JASP¹⁰⁰, with 12 ROIs: left and right CA1, CA3, pmErC, BA36, tErC and PhC. See in refs. 32,30 for similar methods.

The same analyses, but using human subjective ratings of similarity, and layers 3 and 6 of AlexNet are presented in Supplementary Results.

Resting-state functional connectivity analyses

Seed-based connectivity. Seed-based connectivity maps were estimated, characterising the spatial pattern of functional connectivity with a seed area while controlling for all other seeds. Seed regions included the 12 ROIs from the MTL. Functional connectivity strength was represented by Fisher-transformed semi-partial ICC (thus allowing controlling for any signal bleed between adjacent regions) from a weighted general linear model (GLM), estimated separately for each target voxel, modelling the association between all seeds simultaneously and each individual voxel BOLD signal timeseries. To compensate for possible transient magnetisation effects at the beginning of each run, individual scans were weighted by a step function convolved with an SPM canonical hemodynamic response function and rectified.

Then, group-level analyses were performed using a GLM. For each individual voxel, a separate GLM was estimated, with first-level connectivity measures at this voxel as dependent variables and participant's ID as independent variable. Voxel-level hypotheses were evaluated using multivariate parametric statistics with random-effects across subjects and sample covariance estimation across multiple measurements. Inferences were performed at the level of individual clusters (groups of contiguous voxels). Cluster-level inferences were based on parametric statistics from Gaussian Random Field theory¹⁰⁵. Results were thresholded using a combination of a cluster-forming $p < 0.001$ voxel-level threshold, and a familywise corrected p FDR < 0.05 cluster-size threshold¹⁰⁶. Subsequently, contrasts were run between the first-level connectivity measures associated with sensitivity to visual similarity indices in the objects versus scenes conditions, separately for the odd-one-out and the recognition memory task.

ROI-to-ROI functional connectivity. In the first-level analysis, ROI-to-ROI connectivity matrices were estimated for each participant to characterise the functional connectivity between each pair of regions, including the 12 ROIs from the MTL, as well as additional ROIs belonging to the PM-AT systems (29 ROIs in total, see Fig. 5). Functional connectivity strength was represented by Fisher-transformed semi-partial correlations, which allowed controlling for any signal bleed between adjacent regions. Coefficients from a weighted-GLM were estimated separately for each pair of ROIs, which characterised the association between their BOLD signal time series. To compensate for possible transient magnetisation effects at the beginning of each run, individual scans were weighted by a step function convolved with an SPM canonical hemodynamic response function and rectified.

Then, at the group level, a first analysis was performed in CONN using a GLM to characterise the pattern of functional connectivity among all the ROIs. For each individual connection, a separate GLM was estimated, with first-level connectivity measures at this connection as dependent variables and participant's ID as independent variable. Connection-level hypotheses were evaluated using multivariate parametric statistics with random effects across subjects and sample covariance estimation across multiple measurements. Inferences were performed at the level of individual clusters (groups of similar connections). Cluster-level inferences were based on parametric statistics within- and between- each pair of networks¹⁰⁷, with networks identified using a complete-linkage hierarchical clustering procedure based on ROI-to-ROI anatomical proximity and functional similarity metrics. Results were thresholded using a combination of a $p < 0.05$ connection-level threshold and a familywise corrected p FDR < 0.05 cluster-level threshold.

Then, first-level connectivity strength values for each connection and each subject were extracted to perform linear regression analyses with the forward stepwise method, to assess the association between the connections among selected ROIs and the indices of sensitivity to visual similarity, tested one at a time (4 indices in total, derived from object and scene conditions, for both odd-one-out and recognition memory tasks). These analyses were run in JASP¹⁰⁰. To reduce the number of measures entered in the analysis, we ran separate analyses including exclusively regions from the AT system and the hippocampus on one hand (i.e. AT system: bilateral tErC, BA36, superior

frontal gyrus, orbito-frontal cortex, temporal pole, and medial prefrontal cortex; hippocampus: bilateral CA1 and CA3), and of the PM system and the hippocampus on the other hand (i.e. bilateral pmErC, PhC, angular gyrus, superior and inferior lateral occipital cortex, precuneus, thalamus, and PCC). Additionally, we restricted the analyses to selected hypotheses-driven connections involving tErC connectivity and pmErC connectivity, respectively.

Reporting summary

Further information on research design is available in the Nature Portfolio Reporting Summary linked to this article.

Data availability

The dataset¹⁰⁸ is available on the OSF platform, https://osf.io/a5v6k/?view_only=c9f8116f7521469caf727e6db252e691. Raw MRI source data is available on request to the corresponding author.

Code availability

All custom code¹⁰⁸ is available on the OSF platform, https://osf.io/a5v6k/?view_only=c9f8116f7521469caf727e6db252e691.

Received: 22 July 2024; Accepted: 8 May 2025;

Published online: 25 May 2025

References

1. Taylor, K. I. & Probst, A. Anatomic localization of the transentorhinal region of the perirhinal cortex. *Neurobiol. Aging* **29**, 1591–1596 (2008).
2. Braak, H. & Braak, E. Neuropathological staging of Alzheimer-related changes. *Acta Neuropathol.* **82**, 239–259 (1991).
3. Jagust, W. Imaging the evolution and pathophysiology of Alzheimer disease. *Nat. Rev. Neurosci.* **19**, 687–700 (2018).
4. Khan, U. A. et al. Molecular drivers and cortical spread of lateral entorhinal cortex dysfunction in preclinical Alzheimer's disease. *Nat. Neurosci.* **17**, 304–311 (2014).
5. De Flores, R. et al. Contribution of mixed pathology to medial temporal lobe atrophy in Alzheimer's disease. *Alzheimers Dement* **16**, 843–852 (2020).
6. McKhann, G. M. et al. The diagnosis of dementia due to Alzheimer's disease: recommendations from the National Institute on Aging-Alzheimer's Association workgroups on diagnostic guidelines for Alzheimer's disease. *Alzheimers Dement* **7**, 263–269 (2011).
7. Sone, D. et al. Regional tau deposition and subregion atrophy of medial temporal structures in early Alzheimer's disease: a combined positron emission tomography/magnetic resonance imaging study. *Alzheimers Dement. Diagn. Assess. Dis. Monit.* **9**, 35–40 (2017).
8. Whitwell, J. L. et al. MRI correlates of neurofibrillary tangle pathology at autopsy: a voxel-based morphometry study. *Neurology* **71**, 743–749 (2008).
9. Shah, P. et al. Mapping the structural and functional network architecture of the medial temporal lobe using 7T MRI. *Hum. Brain Mapp.* **39**, 851–865 (2018).
10. Dickerson, B. C. & Eichenbaum, H. The episodic memory system: neurocircuitry and disorders. *Neuropsychopharmacology* **35**, 86–104 (2010).
11. Adams, J. N., Maass, A., Harrison, T. M., Baker, S. L. & Jagust, W. J. Cortical tau deposition follows patterns of entorhinal functional connectivity in aging. *eLife* **8**, e49132 (2019).
12. Franzmeier, N. et al. Functional brain architecture is associated with the rate of tau accumulation in Alzheimer's disease. *Nat. Commun.* **11**, 347 (2020).
13. Grajski, K. A. & Bressler, S. L. Differential medial temporal lobe and default-mode network functional connectivity and morphometric changes in Alzheimer's disease. *NeuroImage Clin.* **23**, 101860 (2019).
14. Ossenkoppele, R. et al. Tau covariance patterns in Alzheimer's disease patients match intrinsic connectivity networks in the healthy brain. *NeuroImage Clin.* **23**, 101848 (2019).
15. Berron, D., van Westen, D., Ossenkoppele, R., Strandberg, O. & Hansson, O. Medial temporal lobe connectivity and its associations with cognition in early Alzheimer's disease. *Brain* **143**, 1233–1248 (2020).
16. Hrybowski, S. et al. Aging and Alzheimer's disease have dissociable effects on local and regional medial temporal lobe connectivity. *Brain Commun.* **5**, fcaad245 (2023).
17. Jack, C. R. et al. Tracking pathophysiological processes in Alzheimer's disease: an updated hypothetical model of dynamic biomarkers. *Lancet Neurol.* **12**, 207–216 (2013).
18. Jack, C. R. et al. NIA-AA research framework: toward a biological definition of Alzheimer's disease. *Alzheimers Dement* **14**, 535–562 (2018).
19. Ranganath, C. & Ritchey, M. Two cortical systems for memory-guided behaviour. **15**, 713–26 (2012).
20. Ritchey, M., Libby, L. A. & Ranganath, C. Cortico-hippocampal systems involved in memory and cognition. in *Progress in Brain Research* vol. 219 45–64 (Elsevier, 2015).
21. Cowell, R. A., Barense, M. D. & Sadi, P. S. A Roadmap for understanding memory: decomposing cognitive processes into operations and representations. *eNeuro* **6**, ENEURO.0122-19.2019 (2019).
22. Bussey, T. J., Saksida, L. M. & Murray, E. A. The perceptual-mnemonic/feature conjunction model of perirhinal cortex function. *Q. J. Exp. Psychol. Sect. B* **58**, 269–282 (2005).
23. Bastin, C. et al. An integrative memory model of recollection and familiarity to understand memory deficits. *Behav. Brain Sci.* **42**, e281 (2019).
24. Bastin, C. & Delhay, E. Targeting the function of the transentorhinal cortex to identify early cognitive markers of Alzheimer's disease. *Cogn. Affect. Behav. Neurosci.* <https://doi.org/10.3758/s13415-023-01093-5>. (2023).
25. Besson, G., Simon, J., Salmon, E. & Bastin, C. Familiarity for entities as a sensitive marker of antero-lateral entorhinal atrophy in amnesic mild cognitive impairment. *Cortex* **128**, 61–72 (2020).
26. Gellersen, H. M. et al. Medial temporal lobe structure, mnemonic and perceptual discrimination in healthy older adults and those at risk for mild cognitive impairment. *Neurobiol. Aging* **122**, 88–106 (2023).
27. Yeung, L.-K. et al. Anterolateral entorhinal cortex volume predicted by altered intra-item configural processing. *J. Neurosci.* **37**, 5527–5538 (2017).
28. Westerberg, C. et al. Distinct medial temporal contributions to different forms of recognition in amnesic mild cognitive impairment and Alzheimer's disease. *Neuropsychologia* **51**, 2450–2461 (2013).
29. Westerberg, C. E. et al. When memory does not fail: familiarity-based recognition in mild cognitive impairment and Alzheimer's disease. *Neuropsychology* **20**, 193–205 (2006).
30. Delhay, E., Bahri, M. A., Salmon, E. & Bastin, C. Impaired perceptual integration and memory for unitized representations are associated with perirhinal cortex atrophy in Alzheimer's disease. *Neurobiol. Aging* **73**, 135–144 (2019).
31. Delhay, E. et al. Associative memory for conceptually unitized word pairs in mild cognitive impairment is related to the volume of the perirhinal cortex. *Hippocampus* **29**, 630–638 (2019).
32. Frick, A., Besson, G., Salmon, E. & Delhay, E. Perirhinal cortex is associated with fine-grained discrimination of conceptually confusable objects in Alzheimer's disease. *Neurobiol. Aging* **130**, 1–11 (2023).
33. Kivisaari, S. L., Monsch, A. U. & Taylor, K. I. False positives to confusable objects predict medial temporal lobe atrophy. *Hippocampus* **23**, 832–841 (2013).

34. Joubert, S. et al. The cognitive and neural expression of semantic memory impairment in mild cognitive impairment and early Alzheimer's disease. *Neuropsychologia* **48**, 978–988 (2010).
35. Kivisaari, S. L., Tyler, L. K., Monsch, A. U. & Taylor, K. I. Medial perirhinal cortex disambiguates confusable objects. *Brain* **135**, 3757–3769 (2012).
36. Berron, D. et al. Age-related functional changes in domain-specific medial temporal lobe pathways. *Neurobiol. Aging* **65**, 86–97 (2018).
37. Berron, D. et al. Higher CSF tau levels are related to hippocampal hyperactivity and object mnemonic discrimination in older adults. *J. Neurosci.* **39**, 8788–8797 (2019).
38. Reagh, Z. M. et al. Functional imbalance of anterolateral entorhinal cortex and hippocampal dentate/CA3 underlies age-related object pattern separation deficits. *Neuron* **97**, 1187–1198.e4 (2018).
39. Adams, J. N. et al. Entorhinal–hippocampal circuit integrity is related to mnemonic discrimination and amyloid- β pathology in older adults. *J. Neurosci.* **42**, 8742–8753 (2022).
40. Maass, A. et al. Alzheimer's pathology targets distinct memory networks in the ageing brain. *Brain* **142**, 2492–2509 (2019).
41. Gaynor, L. S. et al. Visual object discrimination impairment as an early predictor of mild cognitive impairment and Alzheimer's disease. *J. Int. Neuropsychol. Soc.* **25**, 688–698 (2019).
42. Jiang, L. et al. Impaired perceptual discrimination of complex objects in older adults at risk for dementia. *Hippocampus* **34**, 197–203 (2024).
43. Mason, E. J. et al. Family history of Alzheimer's disease is associated with impaired perceptual discrimination of novel objects. *J. Alzheimers Dis.* **57**, 735–745 (2017).
44. Newsome, R. N., Duarte, A. & Barense, M. D. Reducing perceptual interference improves visual discrimination in mild cognitive impairment: implications for a model of perirhinal cortex function. *Hippocampus* **22**, 1990–1999 (2012).
45. Cecchini, M. A., Parra, M. A., Brazzelli, M., Logie, R. H. & Della Sala, S. Short-term memory conjunctive binding in Alzheimer's disease: a systematic review and meta-analysis. *Neuropsychology* **37**, 769–789 (2023).
46. Done, D. J. & Hajilou, B. B. Loss of high-level perceptual knowledge of object structure in DAT. *Neuropsychologia* **43**, 60–68 (2005).
47. Barense, M. D., Gaffan, D. & Graham, K. S. The human medial temporal lobe processes online representations of complex objects. *Neuropsychologia* **45**, 2963–2974 (2007).
48. Buckley, M. J., Booth, M. C. A., Rolls, E. T. & Gaffan, D. Selective perceptual impairments after perirhinal cortex ablation. *J. Neurosci.* **21**, 9824–9836 (2001).
49. Devlin, J. T. & Price, C. J. Perirhinal contributions to human visual perception. *Curr. Biol.* **17**, 1484–1488 (2007).
50. Johnson, K. A. et al. Tau positron emission tomographic imaging in aging and early Alzheimer disease. *Ann. Neurol.* **79**, 110–119 (2016).
51. Young, C. B. et al. Divergent cortical tau positron emission tomography patterns among patients with preclinical Alzheimer disease. *JAMA Neurol.* **79**, 592 (2022).
52. Olsen, R. K. et al. Human anterolateral entorhinal cortex volumes are associated with cognitive decline in aging prior to clinical diagnosis. *Neurobiol. Aging* **57**, 195–205 (2017).
53. Clarke, A., Devereux, B. J. & Tyler, L. K. Oscillatory dynamics of perceptual to conceptual transformations in the ventral visual pathway. *J. Cogn. Neurosci.* **30**, 1590–1605 (2018).
54. Devereux, B. J., Clarke, A. & Tyler, L. K. Integrated deep visual and semantic attractor neural networks predict fMRI pattern-information along the ventral object processing pathway. *Sci. Rep.* **8**, 10636 (2018).
55. Krizhevsky, A., Sutskever, I. & Hinton, G. E. ImageNet classification with deep convolutional neural networks. *Adv. Neural Inf. Process. Syst.* **25**, 84–90 (2012).
56. Hovhannisyan, M. et al. The visual and semantic features that predict object memory: concept property norms for 1000 object images. *Mem. Cogn.* **49**, 712–731 (2021).
57. Wright, P., Randall, B., Clarke, A. & Tyler, L. K. The perirhinal cortex and conceptual processing: effects of feature-based statistics following damage to the anterior temporal lobes. *Neuropsychologia* **76**, 192–207 (2015).
58. Yushkevich, P. A. et al. Automated volumetry and regional thickness analysis of hippocampal subfields and medial temporal cortical structures in mild cognitive impairment: automatic Morphometry of MTL Subfields in MCI. *Hum. Brain Mapp.* **36**, 258–287 (2015).
59. Yeung, L.-K. et al. Object-in-place memory predicted by anterolateral entorhinal cortex and parahippocampal cortex volume in older adults. *J. Cogn. Neurosci.* **31**, 711–729 (2019).
60. Berron, D. et al. Early stages of tau pathology and its associations with functional connectivity, atrophy and memory. *Brain* **144**, 2771–2783 (2021).
61. Ferko, K. M. et al. Activity in perirhinal and entorhinal cortex predicts perceived visual similarities among category exemplars with highest precision. *eLife* **11**, e66884 (2022).
62. Knierim, J. J., Neunuebel, J. P. & Deshmukh, S. S. Functional correlates of the lateral and medial entorhinal cortex: objects, path integration and local–global reference frames. *Philos. Trans. R. Soc. B Biol. Sci.* **369**, 20130369 (2014).
63. Schultz, H., Sommer, T. & Peters, J. The role of the human entorhinal cortex in a representational account of memory. *Front. Hum. Neurosci.* **9**, 628 (2015).
64. Clarke, A. & Tyler, L. K. Understanding what we see: how we derive meaning from vision. *Trends Cogn. Sci.* **19**, 677–687 (2015).
65. Jozwik, K. M., Kietzmann, T. C., Cichy, R. M., Kriegeskorte, N. & Mur, M. Deep neural networks and visuo-semantic models explain complementary components of human ventral-stream representational dynamics. *J. Neurosci.* **43**, 1731–1741 (2023).
66. Brady, T. F., Robinson, M. M., Williams, J. R. & Wixted, J. T. Measuring memory is harder than you think: how to avoid problematic measurement practices in memory research. *Psychon. Bull. Rev.* <https://doi.org/10.3758/s13423-022-02179-w> (2022).
67. Besson, G. et al. Fast, but not slow, familiarity is preserved in patients with amnesic mild cognitive impairment. *Cortex* **65**, 36–49 (2015).
68. Olman, C. A., Davachi, L. & Inati, S. Distortion and signal loss in medial temporal lobe. *PLoS ONE* **4**, e8160 (2009).
69. Xu, J. et al. Evaluation of slice accelerations using multiband echo planar imaging at 3T. *NeuroImage* **83**, 991–1001 (2013).
70. Kundu, P. et al. Multi-echo fMRI: a review of applications in fMRI denoising and analysis of BOLD signals. *NeuroImage* **154**, 59–80 (2017).
71. Riddoch, M. J. & Humphreys, G. W. *Borob: Birmingham Object Recognition Battery* <https://doi.org/10.4324/9781003069645>. (Psychology Press, London, 2022).
72. Nasreddine, Z. S. et al. The Montreal Cognitive Assessment, MoCA: a brief screening tool for mild cognitive impairment. *J. Am. Geriatr. Soc.* **53**, 695–699 (2005).
73. Farias, S. T. et al. The measurement of everyday cognition (ECog): scale development and psychometric properties. *Neuropsychology* **22**, 531–544 (2008).
74. Adlington, R. L., Laws, K. R. & Gale, T. M. The Hatfield Image Test (HIT): a new picture test and norms for experimental and clinical use. *J. Clin. Exp. Neuropsychol.* **31**, 731–753 (2009).
75. Brady, T. F., Konkle, T., Alvarez, G. A. & Oliva, A. Visual long-term memory has a massive storage capacity for object details. *Proc. Natl. Acad. Sci. USA* **105**, 14325–14329 (2008).
76. Brodeur, M. B., Guérard, K. & Bouras, M. Bank of Standardized Stimuli (BOSS) Phase II: 930 new normative photos. *PLoS ONE* **9**, e106953 (2014).

77. Konkle, T., Brady, T. F., Alvarez, G. A. & Oliva, A. Conceptual distinctiveness supports detailed visual long-term memory for real-world objects. *J. Exp. Psychol. Gen.* **139**, 558–578 (2010).
78. Kovalenko, L. Y., Chaumon, M. & Busch, N. A. A Pool of Pairs of Related Objects (POPORO) for investigating visual semantic integration: behavioral and electrophysiological validation. *Brain Topogr.* **25**, 272–284 (2012).
79. Moreno-Martínez, F. J. & Montoro, P. R. An Ecological alternative to Snodgrass & vanderwart: 360 high quality colour images with norms for seven psycholinguistic variables. *PLoS ONE* **7**, e37527 (2012).
80. Tarr Lab Object Databank. https://drive.google.com/file/d/1_2H7byO2xSXTOOCZP4zDIHbMPTs5Xlx3/view (1996).
81. Konkle, T., Brady, T. F., Alvarez, G. A. & Oliva, A. Scene memory is more detailed than you think: the role of categories in visual long-term memory. *Psychol. Sci.* **21**, 1551–1556 (2010).
82. Oliva, A. & Torralba, A. Modeling the shape of the scene: a holistic representation of the spatial envelope. *Int. J. Comput. Vis.* **42**, 145–175 (2001).
83. Xiao, J., Ehinger, K. A., Hays, J., Torralba, A. & Oliva, A. SUN database: exploring a large collection of scene categories. *Int. J. Comput. Vis.* **119**, 3–22 (2016).
84. Bruffaerts, R. et al. Redefining the resolution of semantic knowledge in the brain: Advances made by the introduction of models of semantics in neuroimaging. *Neurosci. Biobehav. Rev.* **103**, 3–13 (2019).
85. Zeiler, M. D. & Fergus, R. Visualizing and Understanding Convolutional Networks. in *Computer Vision* 818–833 (Springer International Publishing, 2014).
86. Peirce, J. et al. PsychoPy2: experiments in behavior made easy. *Behav. Res. Methods* **51**, 195–203 (2019).
87. Belyi, N., Guillemin, C., Pommier, E., Hammad, G. & Phillips, C. Bidsme: expandable BIDS-ifier of brain imagery datasets. *J. Open Source Softw.* **8**, 5575 (2023).
88. Shrout, P. E. & Fleiss, J. L. Intraclass correlations: uses in assessing rater reliability. *Psychol. Bull.* **86**, 420–428 (1979).
89. Jenkinson, M., Beckmann, C. F., Behrens, T. E. J., Woolrich, M. W. & Smith, S. M. FSL. *NeuroImage* **62**, 782–790 (2012).
90. Andersson, J. L. R., Hutton, C., Ashburner, J., Turner, R. & Friston, K. Modeling geometric deformations in EPI time series. *NeuroImage* **13**, 903–919 (2001).
91. Ashburner, J. & Friston, K. J. Unified segmentation. *NeuroImage* **26**, 839–851 (2005).
92. Whitfield-Gabrieli, S., Nieto-Castanon, A. & Ghosh, S. Artifact detection tools (ART). *Camb. MA Release Version* **7**, 11 (2011).
93. Nieto-Castanon, A. Preparing fMRI data for statistical analysis. *Arxiv* <https://doi.org/10.48550/arXiv.2210.13564> (2022).
94. Power, J. D. et al. Methods to detect, characterize, and remove motion artifact in resting state fMRI. *NeuroImage* **84**, 320–341 (2014).
95. Nieto-Castanon, A. & Whitfield-Gabrieli, S. *CONN Functional Connectivity Toolbox: RRID SCR_009550, Release 22*. <https://doi.org/10.56441/hilbertpress.2246.5840>. (Hilbert Press, 2022).
96. Whitfield-Gabrieli, S. & Nieto-Castanon, A. Conn: a functional connectivity toolbox for correlated and anticorrelated brain networks. *Brain Connect* **2**, 125–141 (2012).
97. Hallquist, M. N., Hwang, K. & Luna, B. The nuisance of nuisance regression: spectral misspecification in a common approach to resting-state fMRI preprocessing reintroduces noise and obscures functional connectivity. *NeuroImage* **82**, 208–225 (2013).
98. Behzadi, Y., Restom, K., Liao, J. & Liu, T. T. A component based noise correction method (CompCor) for BOLD and perfusion based fMRI. *NeuroImage* **37**, 90–101 (2007).
99. Chai, X. J., Castañón, A. N., Öngür & Whitfield-Gabrieli, D. S. Anticorrelations in resting state networks without global signal regression. *NeuroImage* **59**, 1420–1428 (2012).
100. JASP Team. JASP (Version 0.19.3). [Computer software] (2024).
101. Allaire J.J. *RStudio: Integrated Development for R* (RStudio Team, 2020).
102. Bates, D., Mächler, M., Bolker, B. & Walker, S. Fitting linear mixed-effects models using lme4. *J. Stat. Softw.* **67**, 1–48 (2015).
103. Lenth, R. V. et al. *Estimated marginal means, aka least-squares means* (Scientific research, 2020).
104. Wickham, H. Getting Started with ggplot2. in *ggplot2* 11–31 https://doi.org/10.1007/978-3-319-24277-4_2 (Springer International Publishing, Cham, 2016).
105. Worsley, K. J. et al. A unified statistical approach for determining significant signals in images of cerebral activation. *Hum. Brain Mapp.* **4**, 58–73 (1996).
106. Chumbley, J., Worsley, K., Flandin, G. & Friston, K. Topological FDR for neuroimaging. *NeuroImage* **49**, 3057–3064 (2010).
107. Jafri, M. J., Pearlson, G. D., Stevens, M. & Calhoun, V. D. A method for functional network connectivity among spatially independent resting-state components in schizophrenia. *NeuroImage* **39**, 1666–1681 (2008).
108. Delhay, E., Besson, G., Bahri, M. A. & Bastin, C. Object fine-grained discrimination as a sensitive cognitive marker of transentorhinal integrity. *OSF* <https://doi.org/10.17605/OSF.IO/A5V6K> (2024).

Acknowledgements

The authors thank Dr. David Berron for kindly agreeing to share with us the atlas from his previous work. This work was funded by the FRS-FNRS, the SAO/Fondation Recherche Alzheimer, the Léon Frédéricq Foundation, and the FCT – Fundação para a Ciência e a Tecnologia, I.P., through the Research Center for Psychological Science of the Faculty of Psychology, University of Lisbon (UID/04527: Centro de Investigação em Ciência Psicológica). E.D. was a Postdoctoral Fellow at the F.R.S.-FNRS when the study was conducted. C.B. is a Senior Research Associate at the F.R.S.-FNRS.

Author contributions

E.D.: Conceptualisation, Methodology, Formal analysis, Investigation, Resources, Data Curation, Writing—original draft, Writing—review and editing, Visualisation, Project administration, Funding acquisition; G.B.: Software, Formal analysis, Data Curation, Writing—review and editing, Visualisation; MAB: Software, Formal analysis, Data Curation, Resources, Writing—review and editing; C.B.: Conceptualisation, Resources, Writing—review and editing, Supervision, Project administration, Funding acquisition.

Competing interests

All authors declare no competing interests.

Additional information

Supplementary information The online version contains supplementary material available at <https://doi.org/10.1038/s42003-025-08201-w>.

Correspondence and requests for materials should be addressed to Emma Delhay.

Peer review information *Communications Biology* thanks Pedro Alves and Elisabeth Rounis for their contribution to the peer review of this work. Primary Handling Editors: Michel Thiebaut de Schotten and Benjamin Bessieres. A peer review file is available.

Reprints and permissions information is available at <http://www.nature.com/reprints>

Publisher's note Springer Nature remains neutral with regard to jurisdictional claims in published maps and institutional affiliations.

Open Access This article is licensed under a Creative Commons Attribution-NonCommercial-NoDerivatives 4.0 International License, which permits any non-commercial use, sharing, distribution and reproduction in any medium or format, as long as you give appropriate credit to the original author(s) and the source, provide a link to the Creative Commons licence, and indicate if you modified the licensed material. You do not have permission under this licence to share adapted material derived from this article or parts of it. The images or other third party material in this article are included in the article's Creative Commons licence, unless indicated otherwise in a credit line to the material. If material is not included in the article's Creative Commons licence and your intended use is not permitted by statutory regulation or exceeds the permitted use, you will need to obtain permission directly from the copyright holder. To view a copy of this licence, visit <http://creativecommons.org/licenses/by-nc-nd/4.0/>.

© The Author(s) 2025